Europe PMC Funders Group
Author Manuscript
Nat Chem. Author manuscript; available in PMC 2019 May 26.

Published in final edited form as:
Nat Chem. 2019 January ; 11(1): 32–39. doi:10.1038/s41557-018-0174-9.

Signaling and differentiation in emulsion-based multi-compartmentalized *in vitro* gene circuits

Aurore Dupin and **Friedrich C. Simmel**
Physics Department E14 and ZNN, Technical University Munich, Garching, Germany

Abstract

Multicellularity enables the growth of complex life forms as it allows for specialization of cell types, differentiation, and large scale spatial organization. In a similar way, modular construction of synthetic multicellular systems will lead to dynamic biomimetic materials that can respond to their environment in complex ways. In order to achieve this goal, artificial cellular communication and developmental programs still have to be established. Here, we create geometrically controlled spatial arrangements of emulsion-based artificial cellular compartments containing synthetic *in vitro* gene circuitry, separated by lipid bilayer membranes. We quantitatively determine the membrane pore-dependent response of the circuits to artificial morphogen gradients, which are established via diffusion from dedicated organizer cells. Utilizing different types of feed-forward and feedback *in vitro* gene circuits, we then implement artificial signaling and differentiation processes, demonstrating the potential for the realization of complex spatiotemporal dynamics in artificial multicellular systems.

Keywords

cell-free gene expression; molecular programming; synthetic biology; compartmentalization; artificial cells

The creation of artificial multicellular systems from synthetic cells is an emerging challenge for bottom-up synthetic biology. In biology, the appearance of multicellular systems is regarded as one of the major transitions in the evolution of life on Earth1,2. Multicellularity

Users may view, print, copy, and download text and data-mine the content in such documents, for the purposes of academic research, subject always to the full Conditions of use:http://www.nature.com/authors/editorial_policies/license.html#terms

Author Contributions
A.D. and F.C.S. designed the experiments and wrote the manuscript. A.D. performed the experiments and analyzed the data. A.D. and F.C.S. performed modeling.

Competing Interest
The authors declare no competing financial interests.

Data Availability Statement
Raw data used for the generation of the figures are available from the authors upon request. Plasmids pSB1A3-AD009, pSB1A3-AD010 and pSB1A3-AD011 are available on Addgene.

Code Availability Statement
Custom computer code is used for the analysis of fluorescence videos of the droplets. This involves a routine for tracking the position of moving droplets and fitting the fluorescence data. The code has been used in a previous publication (reference 10 of the Supplementary Information) and is available through a github repository (reference 11 of the Supplementary Information), but also on request from the authors.

Europe PMC Funders Author Manuscripts
Europe PMC Funders Author Manuscripts

Europe PMC Funders Author Manuscripts

Europe PMC Funders Author Manuscripts

enables specialization of cell types and division of labor between cooperating cells, which ultimately results in larger organisms with more diverse capabilities and behaviors than found in unicellular organisms2,3. However, growth of complex multicellular structures and their spatiotemporal organization require sophisticated means of control and cell-to-cell communication. For instance, in the developmental stage of multicellular organisms, gene networks and diffusion gradients induce specification and differentiation of cell types, initiating the generation of global patterns4–6. Similar control systems have to be established for the generation of artificial multicellular structures. Understanding how synthetic *in vitro* gene circuits respond to spatial information will therefore be essential to enable molecular programming of higher order assemblies.

A variety of synthetic biological circuits – both operating *in vitro* and *in vivo* – have been previously employed to create spatiotemporal patterns. *In vivo*, engineered bacteria were demonstrated to produce temporal oscillations in protein expression7 and wave-like phenomena8. Colonies of bacteria endowed with synthetic, quorum sensing-based sender-receiver systems were used for the generation of simple spatial patterns9. Synthetic *in vitro* biochemical circuits have seen major progress recently, either based on the action of only a few enzymes such as RNA or DNA polymerase (the “DNA toolbox”10, genelet11 and RTRACS systems12), or using cell-free gene expression reactions13,14. However, only in a few cases such systems were used to generate spatial patterns15. Of note are the generation of wave-like phenomena16,17, the formation a French Flag pattern18 using the DNA toolbox system, and the establishment of an edge detection system19 via a DNA strand displacement mechanism. Driven by the interest to generate artificial cell-like systems, the dynamics of *in vitro* gene circuits were also studied inside of cell-sized reaction compartments made from liposomes20, in emulsion droplets21–24, or within microfluidic systems25,26, but not considering spatial organization.

Only a few attempts have been made to create artificial structures from multiple compartments. In this context, global communication via quorum sensing signals was studied using liposomes27 or emulsion droplets28,29. “Predatory” behavior was shown in protocell communities composed of coacervates and proteinosomes30. Using the droplet interface bilayer method31,32, multicellular systems were generated, in which artificial cells were connected by protein pores, enabling electrophoretic transfer of molecules between compartments31,33 and light-addressable patterning34. Systems of two or three liposomes sharing a lipid bilayer interface were used to spatially organize enzymatic reactions35 or cell-free protein expression36. More recently, liposomes were utilized to insulate parts of synthetic *in vitro* gene circuits from each other20, and these circuits were executed via globally diffusing chemical signals or vesicle fusion.

Until now, however, there has been no attempt to control the dynamics of *in vitro* gene circuitry in artificial multicellular systems using the positional information provided by chemical gradients. To address this challenge, in the present work we utilized geometrically fixed arrangements of artificial cellular compartments of diameter ≈ 200 μm connected via droplet interface bilayers to implement biomimetic signaling and differentiation processes based on diffusing “morphogens”, which were sent out by dedicated sender droplets. Going beyond simple biochemical signal detection within receiver compartments, we explicitly

Europe PMC Funders Author Manuscripts

Europe PMC Funders Author Manuscripts

used synthetic feedback circuits to sculpt the signaling response of our artificial systems. We first established a toolbox of different circuit environments - genelet circuits11, cell-free gene expression systems, or live bacteria - that could be hosted in the compartments. For direct cell-to-cell signaling, we employed a range of small molecules, which either permeated the bilayers non-specifically, or could pass the membrane interfaces only via protein channels. Based on these components, we then engineered artificial multicellular systems with network-wide signaling and implemented a variety of biomimetic circuits: a diffusion range sensor, a pulse-generating feed-forward circuit, and a positive feedback cell differentiation scheme, demonstrating the potential of this method for engineering complex spatiotemporal dynamics in multicellular assemblies of artificial compartments.

Results

Communicating networks of synthetic cells

We used the droplet interface bilayer (DIB) technique32,37 to connect nanoliter-sized water-in-oil droplets containing synthetic gene circuits into artificial cellular networks (Fig. 1a-d). This technique allows the semi-automated arrangement of assemblies with precise spatial control (Fig. 1b, Supplementary Fig. 1). Although still relatively low-throughput, it could be scaled up, in principle, with a 3D printing technique31. Internal bilayer interfaces restrict the partitioning and diffusion of hydrophilic components, and therefore each compartment attains an identity which is defined by its localized content. To allow for cell-to-cell communication via small hydrophilic signals, we introduced α-hemolysin (α-HL) protein pores38,39 to create water channels across the bilayers. α-HL monomers were encapsulated in targeted droplets and spontaneously assembled into pores in interfaces with neighboring droplets. When diffusion is pore-mediated, small chemicals can only propagate along a path of α-HL containing droplets (Fig. 1c), reaching all the compartments along and adjacent to the path (Fig. 1d, Supplementary Fig. 2 and Supplementary Video 1). Initially identical droplets therefore “differentiate” based on the presence of pores in their neighbors.

The speed of signal propagation through a multicellular system depends on the contributions of the transport processes involved. Within a single compartment (with diameter l), molecules move via diffusion, with the typical time scale for exploration of the compartment given by $t_d = l^2/D$, where D is the diffusivity of the molecules in the aqueous phase. Membrane permeable compounds cross the bilayer with rate $P \cdot \Delta c$, where P is the membrane permeability and Δc the concentration difference across the membrane. The combined effects of free diffusion and membrane permeation can be captured with an “effective” diffusion coefficient, which is given by $D_{eff} = (D^{-1} + (Pl)^{-1})^{-1}$ (cf. Supplementary Text). Thus, for small enough permeabilities and compartment sizes, permeation of the droplet boundaries limits the transport speed. Diffusing chemicals can be trapped inside of a compartment when reacting with macromolecules such as RNA or proteins (Fig. 1e). The diffusion model and transport regimes are described in the Supplementary Text and Supplementary Fig. 3.

Europe PMC Funders Author Manuscripts

Europe PMC Funders Author Manuscripts

Circuit types and molecular signals

We established a variety of reaction environments for the implementation of synthetic gene circuits in multicellular networks (Supplementary Fig. 4): *in vitro* transcriptional circuits11, *in vitro* transcription-translation circuits in bacterial cell extract40, and circuits in live bacterial cells, which differ in their programmability and chemical versatility.

We optimized the lipid composition of the droplet boundaries and the droplet osmolarities (cf. Supplementary Text) to allow for a stable operation of the circuits in the compartments up to several days. Communication between compartments was facilitated by a library of small chemicals, which acted as triggers for synthetic riboregulators or genetic inducers. Depending on their size and chemical nature, the signals propagate via different mechanisms and speeds. For some chemicals, the presence of α-HL pores did not affect inter-compartment diffusion, and we classified this behavior as “non-specific” diffusion (Fig. 2b, Supplementary Fig. 4 and Supplementary Video 2): this was notably the case for the quorum sensing signal C6-HSL (N-(3-Oxohexanoyl)-L-homoserine lactone), for the fluorophore DFHBI and the transcription inducers IPTG (isopropyl β-D-1-thiogalactopyranoside) and aTc (anhydrotetracycline). For other chemicals, permeation through the bilayer was found to be much faster in the presence of α-HL than in its absence (Fig. 2c, Supplementary Fig. 4 and Supplementary Video 1), a behavior we termed “pore-mediated diffusion”: this was the case for the transcription inducers arabinose, rhamnose and DAPG (2,4-Diacetylphloroglucinol), and for guanine (read-out circuits for all the chemicals studied are described in Supplementary Table 1).

Membrane permeability vs. pore-mediated diffusion

Small apolar chemicals usually diffuse “non-specifically” through a lipid bilayer, whereas the diffusion of charged or bulky chemicals is blocked by the correspondingly large free energy barrier. By convention, the partitioning coefficient of a chemical between water and octanol is used as a predictor of the efficiency of partitioning into the bilayer. Other criteria affecting bilayer permeation, such as molecular weight and number of hydrogen bond donors, have been summarized in the so-called Rule of Five41–43, which is employed in pharmacology to assess the druglikeness of a molecule (*i.e.* its ability to permeate cell membranes). Pore-mediated transport of a molecule, on the other hand, depends on the number and diameter of the pores in the bilayer, as well as on interactions between the translocating molecule and the pore’s amino acids.

We used the molecular modeling program Chem3D to calculate the parameters of the Rule of Five (see Supplementary Methods and Supplementary Table 2). Overall, chemicals that satisfied the Rule of Five displayed non-specific diffusion through the bilayer, with DAPG being the only exception. Chemicals that did not satisfy the Rule of Five but had a small enough molecular weight (below ≈ 200 g/mol) were able to diffuse through the α-HL pore. Chemicals not satisfying the Rule of Five and with a high molecular weight were able to diffuse neither through the pores nor through the bilayers: this was the case for transcription inducers lactose and tetracycline.

Europe PMC Funders Author Manuscripts

Europe PMC Funders Author Manuscripts

From the fit of a reaction-diffusion model to our data, we were able to estimate the permeability of the bilayer interfaces to guanine, arabinose, DFHBI and C6-HSL (Supplementary Text, Supplementary Fig. 6 and Supplementary Table 4), which were found to be 8×10^{-10} m·s^{-1}, 5×10^{-8} m·s^{-1}, larger than 9×10^{-6} m·s^{-1} and larger than 2×10^{-6} m·s^{-1}, respectively. For the pore-mediated signals guanine and arabinose, transport through the bilayer was thus found to be the limiting process. By contrast, DFHBI and C6-HSL permeate the lipid membranes very quickly and thus diffusion through the aqueous phase becomes the limiting factor. Overall, the permeability of our networks to the chosen signaling chemicals was found to be comparable to the previously characterized permeabilities of artificial membranes and human red blood cells, which range from around 10^{-7} to 10^{-8} m·s^{-1} for small drug molecules, up to 10^{-5} m·s^{-1} for water and down to 10^{-16} m·s^{-1} for ions44.

Signal propagation through droplet arrays

Detection of a signal diffusing from a sender into a receiver droplet requires the local concentration of the signal molecule to pass over the threshold of the biochemical process that is used for its detection. Signaling range and speed are thus dependent on the initial concentration in the reservoir, the temporally developing diffusion profile and the detection mechanism itself. In order to explore the interplay of these effects, we tested experimentally how the propagation of two genetic inducers with very different permeabilities would affect gene expression in receiver droplets filled with *E. coli* cell extract (Fig. 2a). To this end, three types of compartments were assembled in linear arrays: senders with arabinose and C6-HSL, optional buffer droplets with α-HL pores, and receivers expressing GFP and RFP (specifically mScarletI45) under the control of the corresponding pLux and pBAD promoters. Senders were loaded with inducer concentrations sufficient for full gene induction, resulting in similar steady-state protein expression in bulk (Fig. 2f inset, Supplementary Table 3 and Supplementary Fig. 9 - RFP is delayed with respect to GFP due to slower maturation45,46). When a receiver droplet is brought into contact with the sender without buffer, GFP expression induced by the highly permeable C6-HSL starts immediately and saturates after 2 h, whereas RFP expression is delayed by pore translocation of arabinose and proceeds more slowly than in bulk (Fig. 2f and Supplementary Fig. 7).

In order to gain more intuition on the effect of the permeability on the dynamics of the system, we modeled the signal concentration as a function of time in the receiver droplet for a range of values for P (Fig. 2d). Signal concentrations instantly rise in the receiver for all permeabilities considered, but with very different speeds. The response of an inducible promoter to the rising inducer concentration is shown in Fig. 2e, where we exemplarily assumed an induction threshold of $K_d = 100$ nM and a Hill coefficient of $n = 1.3$ (cooperativity similar to that determined for the pBAD promoter, see Supplementary Fig. 9). A fast (permeable) signal quickly passes the induction threshold and leads to a constant output, whereas slower signals lead to a gradually rising response or – for the slowest signals – no response at all. We thus expected to be able to tune the response to the pore-mediated signal (arabinose) by changing its permeability via the concentration of membrane pores in the buffer droplet. Indeed, RFP expression changes strongly with α-HL concentration, whereas the GFP response (to C6-HSL) is almost unaffected (Fig. 2g).

Europe PMC Funders Author Manuscripts

Europe PMC Funders Author Manuscripts

Alternatively, the signaling response can also be tuned by the number of permeability barriers. When, at constant initial sender concentration, the number of buffer compartments is increased, the final concentration in the droplets and the signaling speed from sender to receiver are reduced. As expected, the response time is more strongly affected for slow diffusing chemicals, as their concentration in the receiver droplet stays well below K_d for sustained periods (Fig. 2h). This effect is confirmed experimentally, with RFP expression dropping significantly with the number of buffer compartments, but GFP expression remaining approximately constant (Fig. 2i, and simulations in Supplementary Fig. 8).

A travelling pulse generated by a feed-forward genelet network

We were next interested in coupling the diffusion of a chemical signal to a compartmentalized chemical reaction network with non-trivial temporal dynamics. For a specific example, we compartmentalized *in vitro* genelet circuits with the topology of an incoherent type-1 feed-forward loop (I1-FFL)47 into a linear array of receiver droplets that were activated by a signal sent out from a sender droplet (Fig. 3a).

In the original I1-FFL motif, an activator gene X activates a response gene Z, but also activates another gene Y which subsequently represses Z, resulting in a transient pulse of expression of Z47. In our genelet implementation, we constructed this motif from sequence-programmable DNA and RNA components (Fig. 3a). As a response readout, we used the Spinach RNA aptamer, which binds the fluorophore DFHBI and thereby strongly increases its fluorescence48. In the initial state of the circuit, the Spinach aptamer is bound to a single-stranded DNA molecule, which has the function of a genelet activator. Upon binding of DFHBI, the ssDNA activator is released and can bind to the incomplete promoter region of a genelet, which acts as the repressor node of the I1-FFL. Activation of the genelet turns on transcription of an RNA molecule, which is fully complementary to the Spinach aptamer. Duplex formation between transcript and Spinach aptamer releases the DFHBI, diminishing its fluorescence again. Hence, in the multi-compartment context, the genelet I1-FFL was expected to create a transient pulse in the concentration of the Spinach/DFHBI complex, which is activated by the diffusing DFHBI “signal” and repressed by the circuit within each compartment.

For the experiment shown in Fig. 3b, we created a linear array of 10 droplets consisting of a trigger droplet containing the “signal molecule” DFHBI connected to a row of nine equal-sized receiver droplets each hosting the same I1-FFL circuit. Connecting the trigger droplet to the nine receiver droplets initiates a fluorescence pulse travelling along the array with an average velocity of ≈ 30 μm/min (Fig. 3b and 3c and Supplementary Video 3). During pulse propagation, fluorescence generated by activation of the Spinach aptamer first steeply rises, followed by a slower attenuation phase caused by the negative feedback of the FFL during which the fluorescence level returns to zero for all but the most distant droplets. By contrast, in a control experiment with DFHBI propagating through an assembly without I1-FFL, the fluorescence level settles at an intermediate level in all droplets (Supplementary Fig. 10).

The speed of the pulse is both determined by the diffusion of the signal and the activity of the genelets. We tuned both parameters by changing the initial DFHBI concentration in the trigger droplet (Fig. 3e) and the amount of T7 RNA polymerase in the receivers (Fig. 3f). As

Europe PMC Funders Author Manuscripts

expected, the pulse indeed becomes faster with more signal and higher transcriptional activity.

The pulse attenuation, on the other hand, depends on the transcriptional activity of the genelets in the respective compartments. As a measure for this activity, we plotted the maximum negative slope of the signal as a function of distance from the source (Fig. 3d). Genelet activity falls steeply up to a distance of ≈ 1 mm (or five compartments) and then slowly decreases towards zero. We interpret the asymptote towards zero as the signaling range of DFHBI, where it falls below the activation threshold of the genelet. In this geometry, the signaling range is approximately 2.8 mm.

To explore further how the geometry of the assemblies affects the dynamics, we assembled 1-dimensional (1D) arrays of 5 receivers and 2-dimensional (2D) arrays of 5x5 receivers in a square layout (Fig. 3g, Supplementary Videos 4 and 5). The signaling range was shortened in the 2D geometry (approximately 1.8 mm) compared to the 1D geometry (approximately 2.6 mm, Fig. 3h). The signaling velocity was faster in 2D than in 1D (Fig. 3i and j), and the velocity in 2D could be similarly tuned with DFHBI and T7 RNA Polymerase concentrations (Fig. 3j). To explore the influence of dimensionality on the pulse, we used a continuous reaction-diffusion model, as permeation of DFHBI through bilayers is not a limiting step. Analysis of the model revealed that the assemblies could not be readily approximated to a 1D or 2D geometry, and that diffusion of the signal in 3D played a role in the dynamics observed. However, the model correctly predicted the overall behavior of the control and pulse experiments, and the range of pulse velocities of this circuit (see Supplementary Text and Supplementary Fig. 11).

Noise-based differentiation of artificial cells

We finally investigated a simple form of “differentiation” of initially identical compartments within our assemblies. In both multicellular and unicellular organisms, stochasticity in biochemical processes is a suggested mechanism of cell differentiation49. For example, fluctuating levels of the mammalian transcription factor Nanog can affect the differentiation behavior of embryonic stem cells50,51. In order to explore similar effects in the context of our cellular assemblies, we engineered a positive feedback circuit to amplify biochemical noise via pore-mediated diffusion. Our circuit is inspired by the *E. coli* lac operon, where the uptake of lactose activates the synthesis of lactose permease LacY, allowing further uptake of lactose and thus stronger activation of the operon52. In our implementation, a gene coding for α-HL monomers and a reporter RFP gene are put under the control of the arabinose-inducible pBAD promoter. The two genes are placed on the same transcript so that the RFP tracks pBAD activation (Fig. 4a). Starting from an initial state without pores in the system, leaky gene expression is expected to lead to the creation of α-HL pores, until the threshold of pore incorporation into the bilayer is crossed. At this point, the membrane permeability for arabinose is increased, further increasing gene activation.

In the experiments, a sender droplet containing arabinose was positioned at the center of a small assembly with four peripheral receivers containing the feedback circuit in *E. coli* cell-extract (Fig. 4b and Supplementary Video 6). We expected that each receiver would produce α-HL with a different leak rate and thus cross the incorporation threshold at a different time

Europe PMC Funders Author Manuscripts

Europe PMC Funders Author Manuscripts

point, breaking the initial symmetry of the system. Indeed, in many of the experiments performed with this system, the receiver compartments displayed a significantly imbalanced RFP expression after 4 hours. The differentiation of the compartments was estimated with the coefficient of variation η of the expression level within each single assembly (standard deviation between all four receivers was divided by their mean). We found that the variability between compartments was often above 20%.

We performed a series of control experiments in order to test whether the observed differentiation in expression levels was significant relative to the baseline variability of protein expression, and also to check the influence of non-specific leaking of arabinose through the membranes (Fig. 4c-e). We found that the mean expression level in the feedback experiment was lower than in a positive control with α-HL present from the beginning, but significantly higher than in negative controls without arabinose or with a truncated construct without the α-HL coding gene (Fig. 4d). This demonstrated that the circuit indeed amplified the initial leak expression that led to the formation of α-HL and created a positive feedback via arabinose influx (cf. also Supplementary Fig. 12 for a control experiment showing dye influx). The negative controls demonstrate that neither leaky expression of the construct, nor leaky diffusion of arabinose can individually account for the protein expression observed in our differentiation experimental conditions.

We also observed that the coefficient of variation η under differentiation conditions was higher on average than in the control conditions (Fig. 4d inset). However, only a fraction of the assemblies noticeably differentiated (η above 20%), suggesting that some assemblies have a homogeneous induction of the positive feedback loop. We fitted the histogram of the variability for each experiment with a lognormal distribution (Fig. 4e) and found that both the mean and the variance of the coefficient of variation were higher in our experiment than in the controls, confirming that the positive feedback loop causes an increase in variability of the protein expression levels. The differentiation observed, although significant, is however not digital.

In order to rationalize this behavior, we modeled systems consisting of sender and receiver droplets accounting for both leaky signal transport and leaky expression and investigated the role of extrinsic noise sources such as variable membrane permeabilities and gene expression strengths (see Supplementary Text). The modeling results suggest that both the differentiation circuit and the positive control are equally sensitive to the extrinsic noise sources. In order to account for the observed higher variability of the differentiation circuit with respect to the control, a considerable variation in membrane incorporation efficiency of the *in situ* generated α-HL pores has to additionally be assumed. This is in line with our observation that the positive feedback receivers reach a given expression threshold at times that are much more broadly distributed than in the control experiments (Supplementary Fig. 13 and 14). In fact, it is known that membrane pore insertion is a relatively inefficient process which strongly depends on α-HL monomer concentration53.

Naively, one could expect that in the assembly with one sender and four receivers, the first receiver droplet that stochastically creates membrane channels will drain the sender droplet from signal before the others gain access to it, and thus lead to a “winner-takes-all” type of

Europe PMC Funders Author Manuscripts

Europe PMC Funders Author Manuscripts

differentiation of the droplets. Our simulations indicate, however, that the four receivers in the system essentially behave the same as four independent receivers. Our model predicts that introduction of a sharper induction threshold could introduce correlations between the four receivers. For low inducer concentrations in the sender droplet, this would result in an enhanced variability in the receivers in the coupled case, but still no clear-cut differentiation (Supplementary Fig. 14). In order to achieve genuine symmetry breaking of the multi-droplet system, more complex feedback circuitry would be required, in which the receiver droplet that is activated first inhibits activation of the other droplets.

Conclusion

We have demonstrated the creation of multi-compartmentalized *in vitro* synthetic biological systems, in which various biochemical functions were distributed and separated in space. This allowed us to emulate basic signaling and differentiation modalities similarly found in multicellular organisms. We first established several inter-compartment signaling pathways based on small molecules, with which we coupled and controlled the dynamics of the gene circuits inside the compartments. Compared to natural signaling processes, the passive diffusion mechanism employed in our artificial assemblies most resembles paracrine signaling, which in nature occurs over a range of tens of cells54 and plays an important role in embryogenesis and differentiation.

Apart from simple control over cell-free transcription and translation processes by artificial morphogen gradients, we also coupled diffusing signals to different types of dynamical *in vitro* circuits within the compartments. In the case of an incoherent transcriptional feed-forward network, this resulted in a transient transcription pulse running through one- and two-dimensional arrays of compartments. In a second example, we created a positive feedback loop that increased membrane permeability by the expression of membrane channels. We found that this circuit creates an increased variability in gene expression levels, giving rise to a primitive form of cellular differentiation.

Our results show that it is possible to employ gradient-based morphogenetic processes in the context of artificial tissues made from physically interconnected artificial cells. Our quantitative analysis of diffusive signaling in such tissues will aid the design of more complex artificial cellular materials in the future, which can sense their chemical environment and that are capable of differentiation based on environmental and positional information. An important feature of compartmentalized systems, which only was hinted at in the present work, is the possibility to combine different and potentially incompatible chemistries in one system. We can therefore envision systems composed of dedicated sensor, information-processing and production cells that can be connected in a modular fashion to achieve a specific function. In combination with additive manufacturing techniques, three-dimensional materials composed of artificial cells with embedded developmental programs will become feasible.

Supplementary Material

Refer to Web version on PubMed Central for supplementary material.

Europe PMC Funders Author Manuscripts

Europe PMC Funders Author Manuscripts

Acknowledgements

This work was supported by the European Research Council (grant agreement no. 694410 - AEDNA) and the DFG Cluster of Excellence Nanosystems Initiative Munich (DFG EXC 4/3). A.D. gratefully acknowledges additional support by the DFG Research Training Group “Chemical Foundations of Synthetic Biology” GRK 2062/1. The authors thank Berta Tinao for her preliminary work on the artificial multicellular assemblies. They also thank Daniela Ziegler and Jonathan List for their help with the set-up construction, Sandra Sagredo and Elisabeth Falgenhauer for providing purified enzymes, and Matthaeus Schwarz-Schilling for helpful discussions. Correspondence and request for materials should be addressed to F.C.S.

References

1. Szathmáry E, Smith JM. The major evolutionary transitions. Nature. 1995; 374:227. [PubMed: 7885442]
2. Grosberg RK, Strathmann RR. The Evolution of Multicellularity: A Minor Major Transition? Annual Review of Ecology, Evolution, and Systematics. 2007; 38:621–654.
3. Bell G, Mooers AO. Size and complexity among multicellular organisms. Biological Journal of the Linnean Society. 1997; 60:345–363.
4. Crick F. Diffusion in Embryogenesis. Nature. 1970; 225:420. [PubMed: 5411117]
5. Christian JL. Morphogen gradients in development: from form to function. Wiley Interdisciplinary Reviews: Developmental Biology. 2012; 1:3–15. [PubMed: 23801664]
6. Green JBA, Sharpe J. Positional information and reaction-diffusion: two big ideas in developmental biology combine. Development. 2015; 142:1203–1211. [PubMed: 25804733]
7. Elowitz MB, Leibler S. A synthetic oscillatory network of transcriptional regulators. Nature. 2000; 403:335–338. [PubMed: 10659856]
8. Danino T, Mondragón-Palomino O, Tsimring L, Hasty J. A synchronized quorum of genetic clocks. Nature. 2010; 463:326–330. [PubMed: 20090747]
9. Basu S, Gerchman Y, Collins CH, Arnold FH, Weiss R. A synthetic multicellular system for programmed pattern formation. Nature. 2005; 434:1130–1134. [PubMed: 15858574]
10. Baccouche A, Montagne K, Padirac A, Fujii T, Rondelez Y. Dynamic DNA-toolbox reaction circuits: a walkthrough. Methods. 2014; 67:234–249. [PubMed: 24495737]
11. Kim J, White KS, Winfree E. Construction of an in vitro bistable circuit from synthetic transcriptional switches. Molecular Systems Biology. 2006; 2
12. Ayukawa S, Takinoue M, Kiga D. RTRACS: a modularized RNA-dependent RNA transcription system with high programmability. Accounts Of Chemical Research. 2011; 44:1369–1379. [PubMed: 22011083]
13. Shin J, Noireaux V. An E. coli Cell-Free Expression Toolbox: Application to Synthetic Gene Circuits and Artificial Cells. ACS Synthetic biology. 2012; 1:29–41. [PubMed: 23651008]
14. Karzbrun E, Tayar AM, Noireaux V, Bar-Ziv RH. Programmable on-chip DNA compartments as artificial cells. Science. 2014; 345:829–832. [PubMed: 25124443]
15. Isalan M, Lemerle C, Serrano L. Engineering Gene Networks to Emulate Drosophila Embryonic Pattern Formation. PLOS Biology. 2005; 3:e64. [PubMed: 15736977]
16. Zadorin AS, Rondelez Y, Galas J-C, Estevez-Torres A. Synthesis of Programmable Reaction-Diffusion Fronts Using DNA Catalyzers. Physical Review Letters. 2015; 114:068301. [PubMed: 25723247]
17. Tayar AM, Karzbrun E, Noireaux V, Bar-Ziv RH. Propagating gene expression fronts in a one-dimensional coupled system of artificial cells. Nature Physics. 2015; 11:1037.
18. Zadorin AS, et al. Synthesis and materialization of a reaction-diffusion French flag pattern. Nature Chemistry. 2017; 9:990–996.
19. Chirieleison SM, Allen PB, Simpson ZB, Ellington AD, Chen X. Pattern transformation with DNA circuits. Nature Chemistry. 2013; 5:1000–1005.
20. Adamala KP, Martin-Alarcon DA, Guthrie-Honea KR, Boyden ES. Engineering genetic circuit interactions within and between synthetic minimal cells. Nature chemistry. 2017; 9:431–439.

Europe PMC Funders Author Manuscripts

21. Hasatani K, et al. High-throughput and long-term observation of compartmentalized biochemical oscillators. Chemical Communications. 2013; 49:8090–8092. [PubMed: 23912586]
22. Weitz M, et al. Diversity in the dynamical behaviour of a compartmentalized programmable biochemical oscillator. Nat Chem. 2014; 6:295–302. [PubMed: 24651195]
23. Genot AJ, et al. High-resolution mapping of bifurcations in nonlinear biochemical circuits. Nature Chemistry. 2016; 8:760.
24. Hansen MMK, et al. Macromolecular crowding creates heterogeneous environments of gene expression in picolitre droplets. Nature Nanotechnology. 2016; 11:191–197.
25. Niederholtmeyer H, et al. Rapid cell-free forward engineering of novel genetic ring oscillators. eLife. 2015; 4
26. Semenov SN, et al. Rational design of functional and tunable oscillating enzymatic networks. Nature Chemistry. 2015; 7:160–165.
27. Lentini R, et al. Integrating artificial with natural cells to translate chemical messages that direct E. coli behaviour. Nature Communications. 2014; 5:4012.
28. Weitz M, et al. Communication and Computation by Bacteria Compartmentalized within Microemulsion Droplets. Journal of the American Chemical Society. 2014; 136:72–75. [PubMed: 24358940]
29. Schwarz-Schilling M, Aufinger L, Muckl A, Simmel FC. Chemical communication between bacteria and cell-free gene expression systems within linear chains of emulsion droplets. Integrative Biology. 2016; 8:564–570. [PubMed: 26778746]
30. Qiao Y, Li M, Booth R, Mann S. Predatory behaviour in synthetic protocell communities. Nature Chemistry. 2016; 9:110–119.
31. Villar G, Graham AD, Bayley H. A Tissue-Like Printed Material. Science. 2013; 340:48–52. [PubMed: 23559243]
32. Thiam AR, Bremond N, Bibette J. From Stability to Permeability of Adhesive Emulsion Bilayers. Langmuir. 2012; 28:6291–6298. [PubMed: 22439743]
33. Yasuga H, et al. Logic Gate Operation by DNA Translocation through Biological Nanopores. PLOS ONE. 2016; 11
34. Booth MJ, Restrepo Schild V, Box SJ, Bayley H. Light-patterning of synthetic tissues with single droplet resolution. Scientific Reports. 2017; 7:9315. [PubMed: 28839174]
35. Elani Y, Law RV, Ces O. Vesicle-based artificial cells as chemical microreactors with spatially segregated reaction pathways. Nat Commun. 2014; 5
36. Elani Y, Law RV, Ces O. Protein synthesis in artificial cells: using compartmentalisation for spatial organisation in vesicle bioreactors. Physical Chemistry Chemical Physics. 2015; 17:15534–15537. [PubMed: 25932977]
37. Bayley H, et al. Droplet interface bilayers. Molecular bioSystems. 2008; 4:1191–1208. [PubMed: 19396383]
38. Song L, et al. Structure of Staphylococcal α-Hemolysin, a Heptameric Transmembrane Pore. Science. 1996; 274:1859–1865. [PubMed: 8943190]
39. Tilley SJ, Saibil HR. The mechanism of pore formation by bacterial toxins. Current Opinion in Structural Biology. 2006; 16:230–236. [PubMed: 16563740]
40. Sun ZZ, et al. Protocols for implementing an Escherichia coli based TX-TL cell-free expression system for synthetic biology. Journal of visualized experiments : JoVE. 2013:e50762. [PubMed: 24084388]
41. Ghose AK, Viswanadhan VN, Wendoloski JJ. A Knowledge-Based Approach in Designing Combinatorial or Medicinal Chemistry Libraries for Drug Discovery. 1. A Qualitative and Quantitative Characterization of Known Drug Databases. Journal of Combinatorial Chemistry. 1999; 1:55–68. [PubMed: 10746014]
42. Petit J, Meurice N, Kaiser C, Maggiora G. Softening the Rule of Five—where to draw the line? Bioorganic & Medicinal Chemistry. 2012; 20:5343–5351. [PubMed: 22222160]
43. Lipinski CA. Rule of five in 2015 and beyond: Target and ligand structural limitations, ligand chemistry structure and drug discovery project decisions. Advanced Drug Delivery Reviews. 2016; 101:34–41. [PubMed: 27154268]

Europe PMC Funders Author Manuscripts

44. Yang NJ, Hinner MJ. Getting Across the Cell Membrane: An Overview for Small Molecules, Peptides, and Proteins. Methods in molecular biology (Clifton, N.J.). 2015; 1266:29–53.
45. Bindels DS, et al. mScarlet: a bright monomeric red fluorescent protein for cellular imaging. Nature Methods. 2016; 14:53. [PubMed: 27869816]
46. Iizuka R, Yamagishi M, Funatsu T. Kinetic Study of De Novo Chromophore Maturation of Fluorescent Proteins. Analytical Biochemistry. 2011; 414:173–178. [PubMed: 21459075]
47. Mangan S, Itzkovitz S, Zaslaver A, Alon U. The Incoherent Feed-forward Loop Accelerates the Response-time of the gal System of Escherichia coli. Journal of Molecular Biology. 2006; 356:1073–1081. [PubMed: 16406067]
48. Paige JS, Wu KY, Jaffrey SR. RNA Mimics of Green Fluorescent Protein. Science. 2011; 333:642–646. [PubMed: 21798953]
49. Eldar A, Elowitz MB. Functional roles for noise in genetic circuits. Nature. 2010; 467:167. [PubMed: 20829787]
50. Chambers I, et al. Nanog safeguards pluripotency and mediates germline development. Nature. 2007; 450:1230. [PubMed: 18097409]
51. Hoffmann M, et al. Noise-Driven Stem Cell and Progenitor Population Dynamics. Plos One. 2008; 3:e2922. [PubMed: 18698344]
52. Ozbudak EM, Thattai M, Lim HN, Shraiman BI, van Oudenaarden A. Multistability in the lactose utilization network of Escherichia coli. Nature. 2004; 427:737. [PubMed: 14973486]
53. Hildebrand A, Pohl M, Bhakdi S. Staphylococcus aureus alpha-toxin. Dual mechanism of binding to target cells. Journal of Biological Chemistry. 1991; 266:17195–17200. [PubMed: 1894613]
54. Müller P, Schier AF. Extracellular movement of signaling molecules. Developmental cell. 2011; 21:145–158. [PubMed: 21763615]

Europe PMC Funders Author Manuscripts

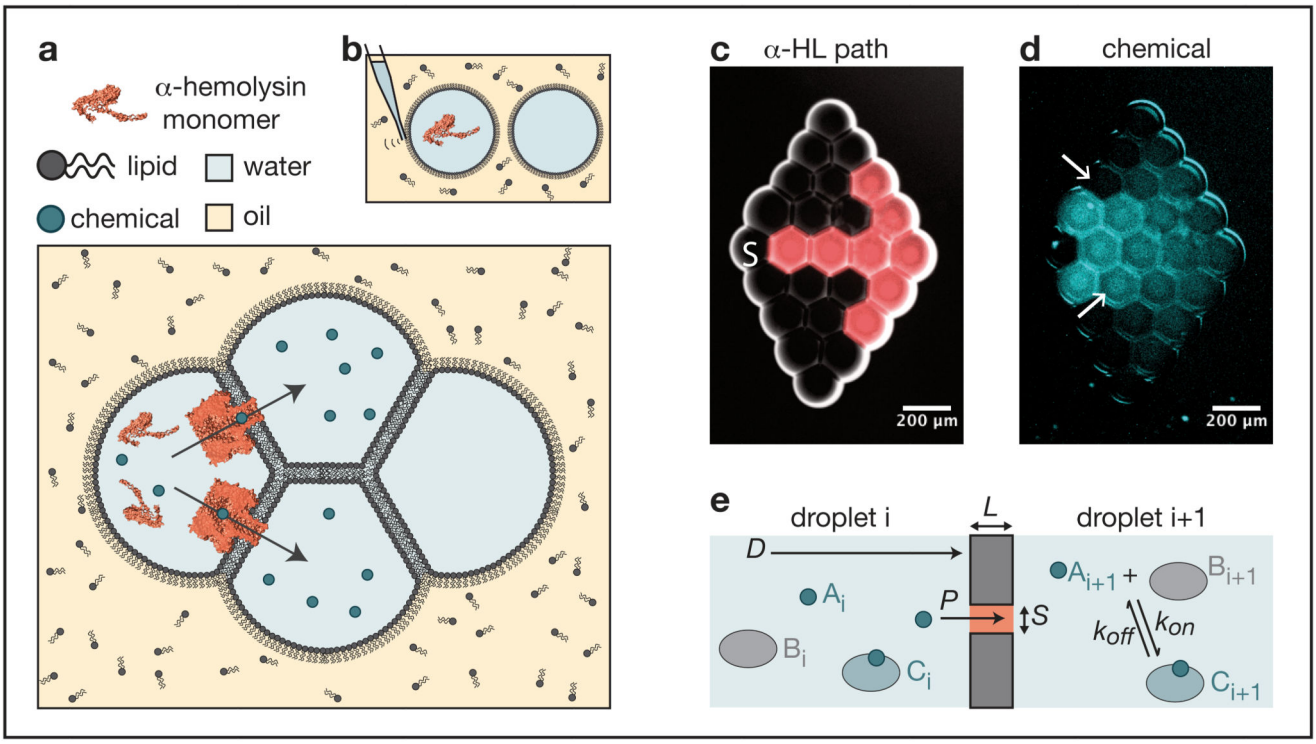

Figure 1. Artificial multicellular structures.

a, Scheme of the networks. Water droplets (blue) are incubated in a lipid-in-oil bath (yellow) where they form bilayers. Protein pores such as α-hemolysin (α-HL, orange) can incorporate into the bilayers and allow the flow of chemicals. **b**, Scheme of the network assembly method: droplets are pipetted and assembled manually with a micromanipulator. **c**, A droplet network is assembled with a sender droplet (S) and receivers containing α-HL (red) or not. **d**, Consequently, a diffusing chemical (blue) can only translocate through bilayers where α-HL is incorporated, and therefore diffuses along the red path and into the direct neighbors. Arrows point to two initially identical droplets, which differentiate based on their environment. Scale bar: 200 μm. **e**, Scheme of the diffusion model, with *D* the diffusivity in aqueous environment, and *P* the permeability of the bilayer of thickness *L*, where pores of cross-section *S* are incorporated. The diffusing species, A, can bind to other species B, switching it to a compartment-trapped state C.

Europe PMC Funders Author Manuscripts
Europe PMC Funders Author Manuscripts

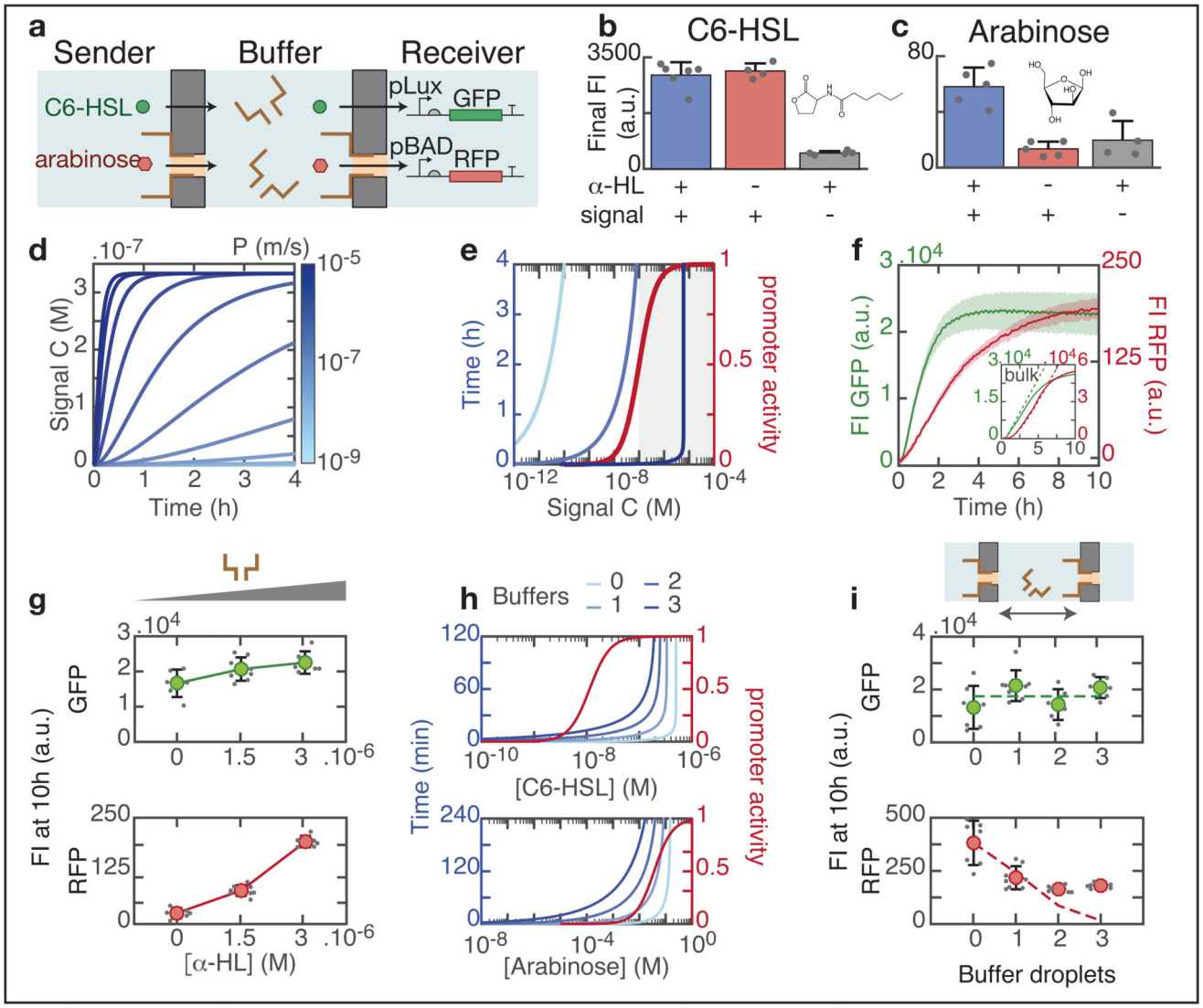

Figure 2. Gene induction by diffusing inducers.

a, Scheme of the experiment: the sender compartment contains C6-HSL and arabinose, the buffer contains pores, and the receiver contains a two-plasmid read-out (GFP under a pLux promoter, RFP under a pBAD promoter). **b, c**, Final fluorescence intensity levels when protein expression is induced by the diffusion of C6-HSL (**b**) and arabinose (**c**), in presence of the chemical and pores (blue), in presence of the chemical and absence of pores (red), and in absence of the chemical but presence of pores (grey). Mean, standard deviation and single data points are plotted. C6-HSL shows a non-specific diffusion, whereas arabinose shows a pore-mediated diffusion. **d**, Simulation of the signal expected in the receiver droplet vs. time for different permeabilities of the bilayer. **e**, Induction of a promoter by a diffusing signal. Left axis, blue: time dependent signal concentration in the receiver for P=10^{-5}, 10^{-7} and 10^{-9} m.s^{-1} (dark blue, median blue and light blue, respectively). Right axis, red: induction curve of a promoter as a function of inducer signal (Hill function with k_d=100 nM, n=1.3). Shaded grey area represents the concentration range where the promoter is induced above 0.5 K_d. **f**,

Europe PMC Funders Author Manuscripts
Europe PMC Funders Author Manuscripts

Mean (full lines) and standard deviation (shaded areas) of the fluorescence intensity of GFP (green) and RFP (red) in a receiver compartment without buffer droplet. Inset: expression in bulk, full lines represent experiment and dotted lines represent simulation. **g**, Mean, standard deviation and single data points of final fluorescence intensities in receiver with varying α-HL concentrations in the buffer droplet. **h**, Simulation of signal concentration in receiver against time, for different number of buffer droplets (blue lines), and induction curve of the corresponding promoter and therefore protein expression (red line). Simulations are conducted with permeabilities, K_d and cooperativities previously determined for C6-HSL and pLux, and for arabinose and pBAD. **i**, Mean, standard deviation and single data points of final fluorescence intensity in receiver with varying number of buffer droplets. Dotted lines represent simulation.

Europe PMC Funders Author Manuscripts

Europe PMC Funders Author Manuscripts

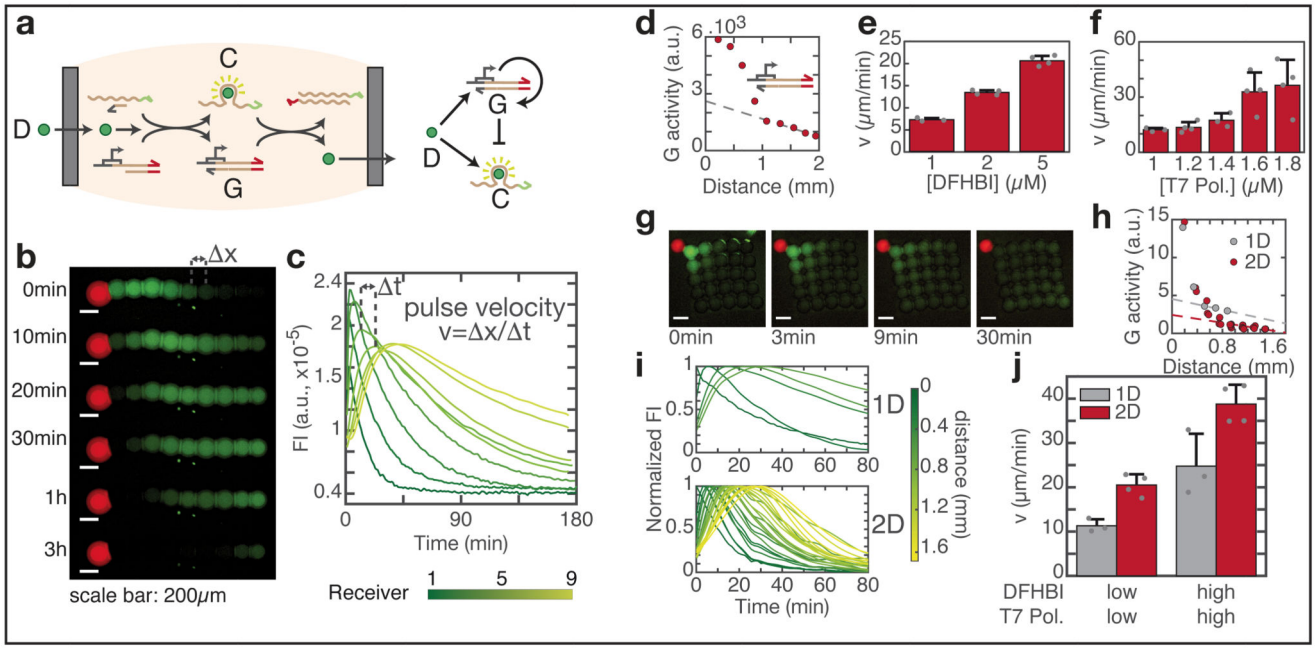

Figure 3. Pulse generation by an incoherent feed-forward loop circuit.

a, Scheme of the pulse circuit. A DFHBI signal diffuses through the assembly. Each receiver droplet contains an RNA (curved line) bound to a ssDNA (straight line), and an incomplete dsDNA template. DFHBI binds the RNA, inducing fluorescence and releasing the ssDNA, which activates the dsDNA template. This is transcribed in an antisense-RNA, which binds the RNA, displaces DFHBI and decreases fluorescence. Right panel shows the simplified circuit as an incoherent feed-forward loop motif. **b**, Propagation of the pulse from a sender droplet (red) to an array of receivers. Fluorescence is shown in green at different time points. Δ*x* indicates the distance between two droplets. Scale bar: 200 μm. **c**, Fluorescence intensity through time for the 9 receivers from **b**. Δ*t* indicates the time between two pulse maxima, and the pulse velocity is calculated by Δ*x*/Δ*t*. **d**, Activity of the dsDNA template G (defined as the maximum negative slope of the fluorescence signal in **c**) depending on distance from the sender (*i.e.*, number of the receiver). Activity decreases as the distance from sender increases, determining the signaling range of the pulse. Dotted line represents linear fit. **e-f**, Mean, standard deviation and single data points of pulse velocity for different DFHBI (**e**) or T7 RNA Polymerase (**f**) concentrations. Velocity can be tuned with those parameters. **g**, Fluorescence image of 2D geometries. The sender is indicated in red, and the fluorescence induced by the circuit is shown in green. Scale bar: 200μm. **h**, Activity of G as a function of the distance from the sender, for 1D and 2D geometries in the same conditions. Dotted lines represent linear fits. **i**, Fluorescence intensity through time for the 1D and the 2D assemblies from **h**. **j**, Velocity compared for 1D and 2D geometries, for slow (low DFHBI, low T7 RNA Polymerase) and fast (high DFHBI, high T7 RNA Polymerase) pulse conditions. Mean, standard deviation and single data points are plotted.

Europe PMC Funders Author Manuscripts
Europe PMC Funders Author Manuscripts

Europe PMC Funders Author Manuscripts

Europe PMC Funders Author Manuscripts

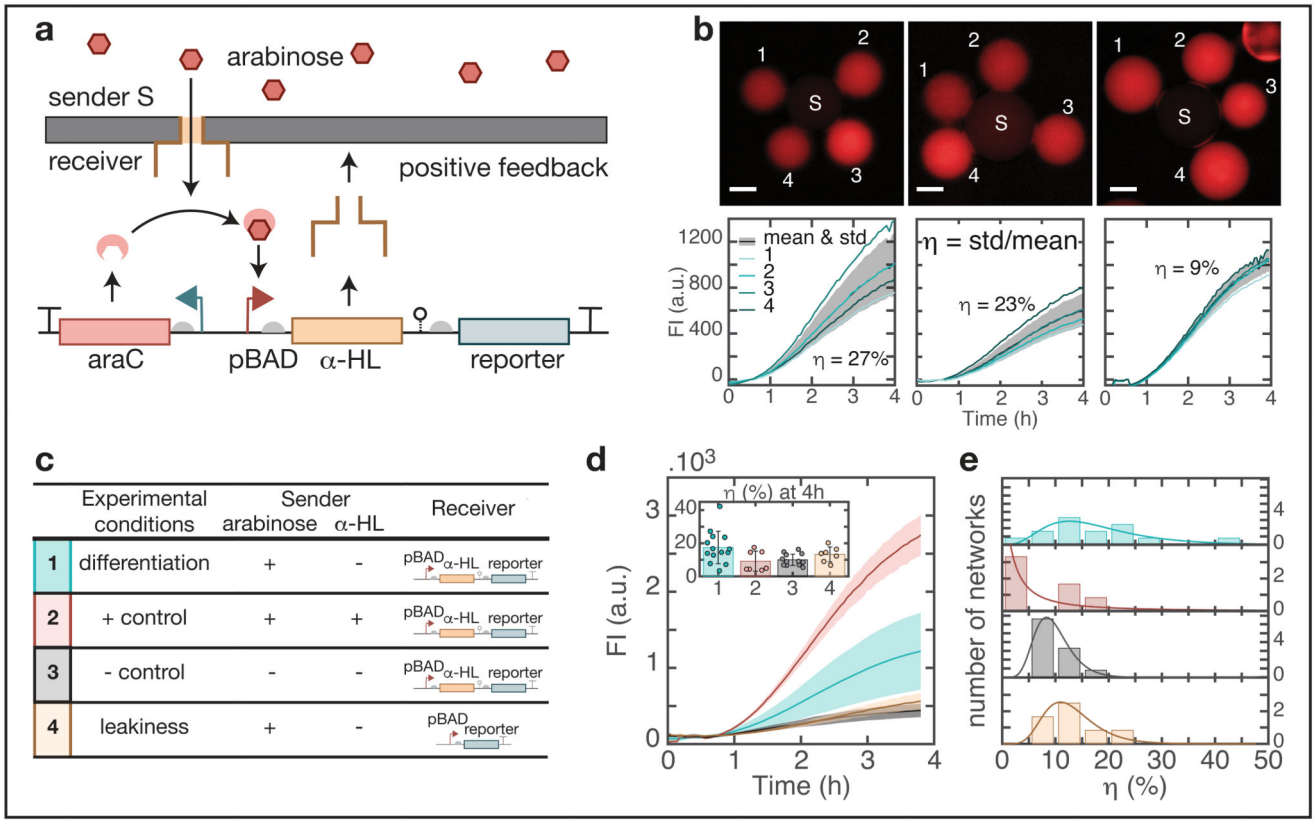

Figure 4. Stochastic differentiation of artificial cells.

a, Scheme of the circuit. The sender contains arabinose (ara). Receivers contain a plasmid with α-HL and a reporter under a pBAD promoter. Leaky transcription of this promoter leads to expression of pores and diffusion of arabinose, creating a positive feedback on pore expression. **b,** Fluorescence images of three different positions, with a sender in the center and receivers on the edges, displaying differentiated protein expression levels, and the corresponding time traces below. The coefficient of variation η of protein expression in the assembly (the standard deviation of all droplets divided by their mean) is indicated in percentage and gives an estimate of differentiation. The left two panels show assemblies with high differentiation, and the right panel shows an assembly with comparatively less differentiation, all three in experimental conditions 1. Scale bar: 100 μm. **c,** Table of the four experimental conditions compared: differentiation experiment in blue, positive control in red, where the promoter is fully induced, negative control in grey where the promoter is not induced, and leakiness control in yellow, where no pores are expressed. **d,** Time traces of the four experiments. Full lines represent mean of all assemblies tested under one experimental condition, shaded areas represent standard deviation. Inset: variability (standard deviation divided by mean) at 4 hours. Dots represent the variability in each assembly. Bar and error bar represent the mean and standard deviation of the variability of all assemblies. **e,** Histogram of the variability of all assemblies in each experimental condition (bars), overlaid with a log-normal fit (continuous line).